The sensitivity of the Greenland ice sheet to glacial-interglacial oceanic forcing

Ilaria Tabone[1,2], Javier Blasco[1,2], Alexander Robinson[1,2,3], Jorge Alvarez-Solas[1,2], and Marisa Montoya[1,2]

[1]Universidad Complutense de Madrid, 28040 Madrid, Spain
[2]Instituto de Geociencias, Consejo Superior de Investigaciones Cientificas-Universidad Complutense de Madrid, 28040 Madrid, Spain
[3]Now at: Faculty of Geology and Geoenvironment, University of Athens, 15784 Athens, Greece

Correspondence to: Ilaria Tabone (itabone@ucm.es)

Abstract. Observations suggest that during the last decades the Greenland Ice Sheet (GrIS) has experienced a gradually accelerating mass loss, in part due to the observed acceleration of several of Greenland's marine-terminating glaciers. Recent studies directly attribute this to increasing North Atlantic temperatures, which have triggered melting of the GrIS outlet glaciers, grounding-line retreat and enhanced ice discharge into the ocean, contributing to an acceleration of sea level rise. Reconstructions suggest that the influence of the ocean has been of primary importance in the past as well. This was the case not only in interglacial periods, when warmer climates led to a rapid retreat of the GrIS to land above sea level, but also in glacial periods, when the GrIS expanded as far as the continental shelf break, and was thus more directly exposed to ocean changes. However, the GrIS response to paleo oceanic variations has not been investigated from a modelling perspective so far. In this work the evolution of the GrIS over the past two glacial cycles has been studied using a three-dimensional hybrid ice-sheet/ice-shelf model. We assess the effect of the variation of oceanic temperatures on the GrIS evolution on glacial-interglacial timescales through changes in submarine melting. The results show a very high sensitivity of the GrIS to the changing oceanic conditions. Oceanic forcing is found to be the dominant driver of the GrIS expansion in glacial times and retreat in interglacial periods. If switched off, paleo atmospheric variations alone are not able to yield a reliable glacial configuration of the GrIS. This work therefore suggests that considering the ocean as an active forcing should become standard in paleo ice sheet modelling.

1 Introduction

Recent observations show that the Greenland Ice Sheet (GrIS) has lost mass at an accelerated rate over the past decades (Rignot et al., 2011; Sasgen et al., 2012; Shepherd et al., 2012; van den Broeke et al., 2016; Zwally et al., 2011). This led the GrIS to contribute to sea level rise on average by $0.47 \pm 0.23 \ \mathrm{mm \, a^{-1}}$ from 1991 to 2015 (van den Broeke et al., 2016), with an accelerated rate of $0.89 \pm 0.09 \ \mathrm{mm \, a^{-1}}$ from 2010 to 2014 (Yi et al., 2015). In the future, the GrIS is expected to continue losing mass, contributing to a sea-level rise relative to the 21th century between 90 and 280 mm by 2100 in the worst-case scenario (RCP8.5) (Bindschadler et al., 2013; Church et al., 2013; Clark et al., 2015; Fürst et al., 2015). This accelerated ice loss is due to a combination of increased surface melting and enhanced ice discharge from marine-terminating glaciers to the ocean (van den Broeke et al., 2016). High surface melting has been attributed to rising atmospheric Greenland temperatures

(Box et al., 2009; Hall et al., 2008; Tedesco et al., 2016), which may also increase crevassing and calving at the ice front. Conversely, the recently enhanced discharge of ice into the ocean is thought to be directly connected to warmer Atlantic waters entering Greenland's fjords (Holland et al., 2008a; Rignot et al., 2010; Straneo et al., 2010; Straneo and Heimbach, 2013). Higher oceanic temperatures increase the submarine melting at the calving front of tidewater glaciers, contributing to their

5   acceleration, ice mass discharge into the ocean and potentially grounding line retreat. This acceleration-and-retreat mechanism has been found in several Greenland glaciers that terminate in the ocean (Rignot and Kanagaratnam, 2006). Jakobshavn Isbrae, West Greenland's fastest glacier, experienced a high rate of basal melting (Motyka et al., 2011) initially induced by the intrusion of warmer waters from the Irminger Sea (Holland et al., 2008a), more than doubling its speed in the last decade and a half (Joughin et al., 2012) and ~~being exposed to a~~ rapid retreat of its terminus. Following enhanced subglacial melting observed in

10   the early 2000s, the Helheim glacier (Southeast Greenland) also doubled its speed (Howat et al., 2005; Sutherland and Straneo, 2012) and suffered peak thinning rates of $90 \, \mathrm{m \, a^{-1}}$ (Stearns and Hamilton, 2007), with its terminus retreating by about 7 km over just 3 years (Howat et al., 2007; Straneo et al., 2016).

The complex mechanisms that lead to ice-shelf thinning, loss of buttressing and potential grounding-line instability have been studied largely for the Antarctic Ice Sheet (AIS) (DeConto and Pollard, 2016; Favier et al., 2014; Hanna et al., 2013; Joughin

15   et al., 2014a; Pritchard et al., 2012; Rignot et al., 2004; Shepherd et al., 2004; Wouters et al., 2015). The thinning of the Larsen C ice-shelf (Holland et al., 2015) and its recent calving event (Hogg and Gudmundsson, 2017; Jansen et al., 2015), the collapse of Larsen B and the melting of the Antarctic Peninsula glaciers (Cook et al., 2016), the widespread retreat of Pine Island and other glaciers in West Antarctica (Alley et al., 2015; Joughin et al., 2014b; Rignot et al., 2014) and the thinning of some East Antarctica ice-shelves (Rignot et al., 2013) are notable examples of the direct connection between changes in oceanic forcing

20   and glacier-termini adjustment (Alley et al., 2015). Only in the last several years has the scientific community also focused its attention on the ice-ocean interaction in Greenland, motivated by the observed acceleration and retreat of major GrIS outlet glaciers. Although marine-terminating glaciers cover only a small fraction of the entire GrIS, modifications at the ice-ocean boundaries due to oceanic changes may considerably affect the inland ice geometry. The effects induced by the outlet-glacier acceleration are transferred onshore by ice-flow dynamics, causing adjustments to the entire inland ice-mass configuration

25   (Nick et al., 2009; Fürst et al., 2013; Golledge et al., 2012). For this reason a full understanding of the interaction between ice and ocean is crucial to assess the response of the GrIS to past and future climate changes.

Various numerical models have been used to simulate current submarine melt rates (Jenkins, 2011; Rignot et al., 2016; Sciascia et al., 2013; Xu et al., 2012, 2013) and dynamic retreat (Morlighem et al., 2016; Vieli and Nick, 2011) of the GrIS marine-terminating glaciers, as well as ice-dynamic future projections of the whole GrIS (Fürst et al., 2015; Nowicki et al., 2013), due

30   to changes in the oceanic temperatures. However, how this thermal forcing affected the past GrIS configuration has not been explored from a modelling perspective so far. Several studies reconstructed the GrIS past evolution as driven essentially by atmospheric forcing (Langebroek and Nisancioglu, 2016; Quiquet et al., 2012, 2013; Robinson et al., 2011; Stone et al., 2013), while, the dynamic evolution of the entire GrIS under the influence of the past oceanic forcing too has only been investigated in a simplified manner. To this end, Huybrechts (2002) used a three-dimensional ice-sheet model in which past basal melting rate

35   variations at the base of the ice shelves follow paleo atmospheric temperature changes with a relaxation time of 100 a, while

Tarasov and Peltier (2002), Simpson et al. (2009) and Lecavalier et al. (2014) performed a paleo reconstruction of the entire GrIS constraining their ice-sheet models with past Relative Sea Level (RSL) reconstructions. However, submarine melting was not taken into account as active forcing in either study.

The main purpose of this work is to assess the impact of ice-ocean interaction on the evolution of the whole GrIS throughout the

5   last glacial cycle. By implementing a submarine melting rate parametrisation suitable for paleoclimatic studies into a 3D hybrid ice-sheet model, we evaluate the sensitivity of the GrIS to past climatic variations, including changes in oceanic temperatures (in terms of heat-flux variations) and we investigate their capability to trigger grounding line expansion and retreat through time.

The paper is structured as follows. First we describe the ice-sheet/ice-shelf model used to simulate the GrIS evolution, focusing

10 on the implemented submarine melt rate parametrisation, and the sensitivity tests performed for this study (Sect. 2). In Section 3 we show the results obtained in each experiment and we compare them with data for the Last Interglacial (LIG), the Last Glacial Maximum (LGM) and the present day found in literature. After considering the main model uncertainties and caveats (Sect. 4), we summarize the main conclusions of this work (Sect. 5).

2   Model description and experimental design

15 ### 2.1   Model

To investigate the oceanic sensitivity of the GrIS throughout the last two glacial cycles we use the three-dimensional, hybrid, ice-sheet/ice-shelf model GRISLI-UCM. The model is an extension of the GRISLI ice-sheet model (Ritz et al., 2001), which has already been succesfully used to simulate the evolution of the past Greenland (Quiquet et al., 2012, 2013) and Antarctic ice sheets (Ritz et al., 2001; Philippon et al., 2006; Alvarez-Solas et al., 2010), as well as the Laurentide ice sheet (Alvarez-Solas

20 et al., 2011, 2013). GRISLI-UCM combines the Shallow Ice Approximation (SIA) for slow inland deformational flow and the Shallow Shelf Approximation (SSA) over fast flowing areas, that is, ice streams and ice shelves, where plug flow is dominant. Since we assume deformational ice sheet regions to be frozen at the bedrock, no basal sliding is considered for SIA dominated areas. Basal sliding for ice streams is determined through a basal drag term ($\boldsymbol{\tau}_b$), defined as a function of the effective pressure (N_{eff}) and the basal horizontal velocity ($\boldsymbol{u}_b$), is considered as follows

25 $$\boldsymbol{\tau}_b = -\beta \, \boldsymbol{u}_b \tag{1}$$

where

$$\beta \propto N_{eff} \tag{2}$$

Dragging at the floating ice shelf base is considered to be zero. The position of the grounding line is evaluated following a flotation criterion based on the current sea level and the ice thickness. The entire GrIS ice dynamics is solved on a computa-

30 tional grid of 20 km x 20 km horizontal resolution and 21 vertical layers. The isostatic adjustment is described by the elastic lithosphere-relaxed asthenosphere method (Le Meur and Huybrechts, 1996), for which the viscous asthenosphere responds to

the ice load with a tunable characteristic relaxation time (see Sect. 2.4).

The hybrid scheme uses a weighting function to combine the non-sliding horizontal SIA velocities ($\boldsymbol{u}_{\text{SIA}}$) with the SSA horizontal velocities ($\boldsymbol{u}_{\text{SSA}}$), and is defined as (Bueler and Brown, 2009):

$$\boldsymbol{u} = (1 - f(u_{\text{SSA}}))\,\boldsymbol{u}_{\text{SIA}} + f(u_{\text{SSA}})\,\boldsymbol{u}_{\text{SSA}} \qquad (3)$$

5 where the weighting function $f(u_{\text{SSA}})$ depends on the module of the SSA component ($\boldsymbol{u}_{\text{SSA}}$) through

$$f(u_{\text{SSA}}) = \frac{2}{\pi}\,arctan\left(\frac{u_{\text{SSA}}}{u_{\text{ref}}}\right)^2 \qquad (4)$$

ranging between 0 and 1. In this work the reference velocity u_{ref} is set to $100\ \text{m a}^{-1}$. For small values of u_{SSA}, $f(u_{\text{SSA}}) \approx 0$ and the horizontal velocities are calculated within the SIA, while $f(u_{\text{SSA}}) \approx 1$ for $u_{\text{SSA}} \gg u_{\text{ref}}$, for which the contribution of SSA dominates.

2.2 Atmospheric forcing

The surface mass balance (SMB) is calculated by the positive degree-day (PDD) scheme (Reeh, 1989) forced by surface atmospheric temperatures and precipitation. This melting scheme is admittedly too simple for paleo simulations (Robinson and Goelzer, 2014), however it is sufficient for the sensitivity experiments performed in this study. The atmospheric temperature

15 forcing is retrieved using a index-anomaly approach in which the present-day climatological field ($T_{\text{clim, atm}}$) is perturbed by past temperature anomalies derived through a spatially-uniform climatic index $\alpha(t)$ (Fig. 1), as follows:

$$T_{\text{atm}}(t) = T_{\text{clim, atm}} + (1 - \alpha(t))\,(T_{\text{LGM, atm}} - T_{\text{PD, atm}}) \qquad (5)$$

The index $\alpha(t)$ is built through a multi-proxy approach. First we combine the temperature reconstruction for Greenland by Vinther et al. (2009) from 11.7 ka BP to present, the NGRIP reconstruction (Kindler et al., 2014) for 115-11.7 ka BP, the

20 NEEM reconstruction (NEEM, 2013) for 135-115 ka BP and we generate a synthetic temperature anomaly time series for the time period 250-135 ka BP following Barker et al. (2011). Second, the signal undergoes a windowed low-pass frequency filter (f_{c} = 1/16 ka^{-1}) in order to remove the spectral components associated with millennial time scales and below. Finally, the index α is obtained by normalizing the resulting signal to be in agreement with Eq. 5, i.e. $\alpha = 0$ at the Last Glacial Maximum (LGM) and $\alpha = 1$ at the present day. The present-day climatological fields are taken from the regional climate model MAR

25 forced by ERA-Interim (Fettweis et al., 2013). $T_{\text{LGM, atm}} - T_{\text{PD, atm}}$ is the Surface Atmospheric Temperature (SAT) difference between the LGM and the present, as simulated by the climatic model of intermediate complexity CLIMBER-3α (Montoya and Levermann, 2008). For the precipitation rate the procedure is similar, but the annual present-day precipitation is scaled by the ratio of the past precipitation to its present value (Banderas et al., 2017).

At the base of the grounded ice, the melt rate is calculated as function of the geothermal heat flux, which is prescribed (Shapiro

30 and Ritzwoller, 2004), and the local pressure melting point. The submarine melt rate is described in detail in the next subsection.

2.3 Oceanic forcing

Several marine basal melting rate parametrisations can be found in the literature. Generally, the submarine melt rate is thought to be directly influenced by the oceanic temperature variations below the ice shelves. Accordingly, most basal melting parametrisations are built as function of the difference between the oceanic temperature at the ice-ocean boundary layer and the temperature at the ice-shelf base, generally assumed to be at the freezing point. The dependence on this temperature difference can be linear (Beckmann and Goosse, 2003) or quadratic (Holland et al., 2008b; Pollard and DeConto, 2012; DeConto and Pollard, 2016; Pattyn, 2017). Because of the increasing temperature anomaly approaching the onshore ice-shelf limit, both schemes ensure a higher basal melting rate close to the grounding line, as suggested by observations (Dutrieux et al., 2013; Rignot and Jacobs, 2002; Wilson et al., 2017).

The marine basal melting rate parametrisation used in this work follows a linear approach that accounts separately for sub-ice shelf areas near the grounding line and for purely floating ice (ice shelves). Following Beckmann and Goosse (2003) the net basal melt rate B_{gl} [m a^{-1}] for ice-shelf cavities close to the grounding line and terminating in shallow ocean zones can be expressed as

$$B_{\mathrm{gl}}(t) = \kappa \left(T_{\mathrm{ocn}}(t) - T_{\mathrm{f}}\right) \tag{6}$$

where T_{ocn} is the oceanic temperature close to the grounding line [K], T_{f} is the temperature at the ice base, assumed to be at the freezing point [K] and κ is the heat flux exchanged between ocean water and ice at the ice-ocean interface [m a^{-1} K^{-1}]. A suitable representation of the transient oceanic temperature T_{ocn} can be given by the climatological oceanic temperature $T_{\mathrm{clim, ocn}}$ corrected by the LGM-present temperature anomaly $(T_{\mathrm{LGM, ocn}} - T_{\mathrm{PD, ocn}})$ scaled by the same climatic-index $\alpha(t)$ used to correct the atmospheric climatological fields (Fig. 1). Under this assumption, Eq. (6) can be rewritten as

$$B_{\mathrm{gl}}(t) = \kappa \left(T_{\mathrm{clim, ocn}} + \Delta T_{\mathrm{ocn}}(t) - T_{\mathrm{f}}\right) \tag{7}$$

where

$$\Delta T_{\mathrm{ocn}}(t) = \left(1 - \alpha(t)\right)\left(T_{\mathrm{LGM, ocn}} - T_{\mathrm{PD, ocn}}\right) \tag{8}$$

Combining and rearranging these equation as

$$B_{\mathrm{gl}}(t) = \kappa \left(T_{\mathrm{clim, ocn}} - T_{\mathrm{f}}\right) + \kappa \, \Delta T_{\mathrm{ocn}}(t) \tag{9}$$

we can finally express the basal melting rate at the grounding line B_{gl} [m a^{-1}] as

$$B_{\mathrm{gl}}(t) = B_{\mathrm{ref}} + \kappa \, \Delta T_{\mathrm{ocn}}(t) \tag{10}$$

The first term B_{ref} [m a^{-1}] is assumed to represent the present-day basal melting rate around the ice sheet and tuned to reproduce the present ice distribution, κ represents the sensitivity of the basal melting rate to changes in the oceanic temperature, and ΔT_{ocn} [K] expresses the temporal evolution of the melting at the ice base. In this way, B_{gl} coincides with its present-day

value (B_{ref}) for $\alpha = 1$ and its LGM (21 ka BP) value for $\alpha = 0$. When B_{gl} is negative, the model allows for refreezing and the grounding line can advance offshore. A variation in κ or an equivalent change in ΔT_{ocn} equally affect the oceanic forcing applied to the model. For the sake of simplicity the glacial-interglacial temperature anomaly $T_{\text{LGM, ocn}} - T_{\text{PD, ocn}}$ (Eq. 8) is assumed here to be spatially constant and set to -3°, which corresponds to the mean value of the reconstructed LGM Sea

5 Surface Temperature (SST) anomalies for the Atlantic Ocean between $60^\circ N$ and $80^\circ N$ of latitude (MARGO, 2009).

The basal melting rate for purely floating ice shelves (B_{sh}) is given by the grounding-line basal melt B_{gl} scaled by a constant factor γ

$$B_{\text{sh}}(t) = \gamma \, B_{\text{gl}}(t) \tag{11}$$

In this study, γ is set to 0.1. With this value set we consider that the basal melting rate for ice shelves is ten times lower than

10 that close to the grounding zone, as in agreement with observations (Rignot and Jacobs, 2002). Conversely, the melt rate in the open ocean, that is considered as beyond the continental shelf break, is prescribed to a high value ($50 \, \text{m a}^{-1}$) to avoid irrealistic ice growth beyond reasonable boundaries.

2.4 Experimental design

15 To study how oceanic changes impact the evolution of the GrIS over the last glacial cycles, we performed a set of sensitivity tests by perturbing the two key parameters of the basal melting rate equation (Eq. 10): the estimated present-day submarine melting B_{ref} and the heat-flux coefficient κ. For each experiment we ran an ensemble of simulations over the GrIS domain throughout the last 250 ka. In this study the model is initialised by the present-day Greenland topography (Bamber et al., 2013), the characteristic relaxation time for the lythosphere is set to 3 ka and the sea level is mantained constant in time at its

20 present-day value. The first ~ 100 ka of the simulation are considered as a spin-up and are not analyzed. A summary of all the parameter values used in each sensitivity test is shown in Table 1.

First, we analyse the sensitivity of the model to different constant (in space and time) reference submarine melting rates B_{ref} applied at the base of the ice-sheet marine margins. Due to the scarcity of submarine melt observations along the GrIS coasts, and since the only recent estimates have focused on few very rapid tidewater Greenland glaciers (Rignot et al., 2010; Motyka

25 et al., 2011; Straneo et al., 2012; Xu et al., 2013; Enderlin and Howat, 2013; Fried et al., 2015; Rignot et al., 2016) that cannot be representative of the basal melt rate for the entirety of GrIS marine areas, we assume present-day basal melting rates for Greenland comparable to those from Antarctic ice shelves (Rignot et al., 2013). The range of values of B_{ref} is thus set between 0 and $40 \, \text{m a}^{-1}$, while the heat-flux coefficient κ is set zero to make the ocean contribution constant in time.

Second, we study the sensitivity of the GrIS to the basal melt rate sensitivity κ at the ice-ocean interface. The range of tested

30 values for κ is between 0 (expressing a temporally constant basal melting rate) and $20 \, \text{m} \, \text{K}^{-1}$. The choice of this range reflects the inference made by Rignot and Jacobs (2002), that a variation of 1 K in the effective oceanic temperature changes the melt rate by $10 \, \text{m a}^{-1}$ (Eq. 6). The sensitivity test for κ is firstly done for $B_{\text{ref}} = 1 \, \text{m a}^{-1}$ and then for other B_{ref} values to show that the GrIS response to the melting rate sensitivity κ depends on the chosen reference basal melting rate (see Table 1).

3 Results

In this section we present the results for each sensitivity study aiming to ~~comprehensively~~ assess the impact of the ocean on the evolution of the GrIS throughout the two last glacial cycles, especially focusing on the Last Interglacial (LIG), the Last Glacial Maximum (LGM) and the present day (PD) GrIS. The present work involved a total of 132 model simulations, although only

5   the most representative cases for each sensitivity study are discussed.

3.1 Sensitivity to the reference submarine melting

Figure 2 shows the evolution of the grounded ice volume (a) and area (b) for the simulations obtained for different values of the reference melting rate B_{ref} and $\kappa = 0$. In this experiment the maximum ice volume reached at glacial times ranges between 3.2-3.9 million km^3, just 8-32 % higher than the observed present-day ice volume (Bamber et al., 2013), suggesting that under

10 constant oceanic forcing, the GrIS is limited to a configuration close to that of nowadays. The highest glacial ice volume is reached by imposing a null basal melting to the GrIS margins ($B_{\mathrm{ref}} = 0$), which corresponds to a simulation forced solely by paleo atmospheric variations. The varying SMB throughout the cycles still results in a changing GrIS ice volume over time. However, during glacials all grounded ice remains on land above sea level, and only small ice shelves are able to grow (Fig. 3). For $B_{\mathrm{ref}} > 0$, a positive melt rate is applied to the marine margins of the whole GrIS throughout the cycles. The submarine

15 melting not only inhibits the grounding-line advance during the glacials, but contributes to thin the few marine-terminating glaciers still present, constraining the grounding line further inland, and resulting in a GrIS extent close to the observed present-day configuration (Fig. 3). This mechanism can be quite active still during glacial times, such that the ice volume can be even lower than that simulated at the present (Fig. 2). Note that the ice volume is more sensitive to B_{ref} during the glacials, as during the interglacials the effect of the ocean is limited by the topography of the Greenland itself.

20 Figure 4 shows the distribution of the ice volume (a) and the percentage of grounded points (b) lost during the last two interglacials. Note that ice volumes have been converted to values of Sea Level Equivalent anomaly (m SLE) with respect to the present-day volumes estimated using an ice density of 916.7 $\mathrm{kg\,m}^{-3}$, a density of the sea water of 1028 $\mathrm{kg\,m}^{-3}$ and a constant ocean area of 3.618 10^8 km^2. Note that the ice loss during the LIG is much higher than for the last deglaciation, as in the LIG the GrIS loses more grounded ice than in the Holocene. For $B_{\mathrm{ref}} < 5$ $\mathrm{m\,a}^{-1}$, the ice lost during the interglacials

25 decreases with increasing B_{ref}, as high basal melting rates inhibit the ice growth in the preceding glacial. For $B_{\mathrm{ref}} > 5$ $\mathrm{m\,a}^{-1}$ both quantities remain constant with respect to B_{ref}. This can easily be explained by the fact that high submarine melting prescribed at the boundaries inhibits the grounding-line advance, resulting in a GrIS that remains totally land-based during glacial periods and implying that any subsequent ice mass loss is uniquely driven by ablation (compare Fig. 3 a and b or Fig. 3 d and e).

3.2 Sensitivity to the heat-flux coefficient

30 Figure 5 shows the glacial-interglacial evolution of the GrIS volume (and area) for different values of the basal melting rate sensitivity κ, having set $B_{\mathrm{ref}} = 1$ $\mathrm{m\,a}^{-1}$. The maximum ice volume simulated in both glacial periods fluctuates between 3.6-5.3 million km^3, greatly exceeding the range found for the case with constant oceanic forcing. Moreover, excluding the experi-

ments with the lowest sensitivities ($\kappa = 0, 0.2$ m a^{-1} K^{-1}), the maximum volume simulated in glacials ranges between 4-5.3 million km^3, i.e. a range of values above the maximum value reached in the B_{ref} sensitivity test. In this particular set of simulations, the GrIS starts to react to the oceanic forcing for $\kappa = 0.5$ m a^{-1} K^{-1}. Ice volume and area during glacials increase, with increasing κ values, as in glacials the negative basal melting rate allows water to freeze favoring ice growth and GrIS expansion. This mechanism is more active for increasing values of κ, which not only lead to more ice loss during interglacials (as easily expected) but induce more ice growth in cold periods too. This behaviour contrasts with what we found for the time-constant oceanic forcing, with ice volume increasing with decreasing B_{ref} both in cold and in warm periods. A larger ice sheet during a glacial maximum loses more ice, leading to an interglacial state that is almost independent of κ. This response is related to the saturation of the oceanic forcing in interglacials, when the GrIS is almost totally land-based and the ice loss thereafter is mostly due to the increasing atmospheric temperature and precipitation. Thus the oceanic sensitivity affects the ice growth in glacials much more than the ice loss during deglaciations.

Figure 6 a-c and Fig. 7 a-c clearly show that the grounding-line advance during glacials depends very strongly on the sensitivity of the ice sheet to oceanic temperature changes. For $\kappa = 0$, as discussed in Section 3.1, the GrIS is constrained to the present-day land area above sea level as the majority of glaciers are land-based. For $\kappa = 1$ m a^{-1} K^{-1} the grounding line has already advanced, expanding from the present-day continental boundaries and generating large ice shelves in the eastern GrIS, especially in the northeast. For $\kappa = 10$ m a^{-1} K^{-1} the GrIS extends all the way to the continental shelf break at its glacial maximum, while only a few small floating ice shelves are present, especially in the East.

These experiments show that the ice loss during the deglaciations monotonically increases with increasing κ (Fig. 8). For a higher κ, more ice grows during glacial periods and more ice is lost faster during the subsequent deglaciation too. For both terminations, the ice volume loss for $\kappa = 20$ m a^{-1} K^{-1} exceeds that lost for $\kappa = 0$ of more than 4 m SLE, i.e. almost two-thirds of the present-day GrIS volume. The significant mass loss in the interglacials is mostly due to the large amount of grounded-ice zones that are converted into ice-free areas during the deglaciation (Fig. 8 b). The percentage of grounded points lost in the deglaciations saturates for κ higher than 5 m a^{-1} K^{-1} in correspondence with glacial GrIS configurations which present a grounding line expansion to the continental shelf break. The slightly increasing ice loss observed for higher oceanic sensitivities is mostly related to the ice lost in the GrIS interiors due to the positive elevation-melt feedback.

Figure 9 shows the ice loss in the Holocene as a function of κ for different values of the reference submarine melting B_{ref} prescribed in the simulations. The magnitude of the sensitivity with respect to κ strictly depends on the value of B_{ref}. The reason for this is that B_{ref} defines the positive threshold that the glacial GrIS has to overcome to start reacting to the oceanic forcing imposed at the margins. For $B_{\mathrm{ref}} = 10$ m a^{-1} the GrIS responds to the ocean only for $\kappa > 4$ m a^{-1} K^{-1}, while for $B_{\mathrm{ref}} = 40$ m a^{-1} the GrIS expands only for $\kappa > 10$ m a^{-1} K^{-1}. Once the reaction has started, the sensitivity of the GrIS to κ increases with increasing B_{ref}, i.e. small variations in the magnitude of κ lead to a fast and large growth of ice during glacials and consequently to a fast and large loss of ice during the deglaciation. Similar results are found for the LIG (not shown).

3.3 Last Interglacial

The amount of ice lost during the LIG depends on the magnitude of the melt rate sensitivity κ imposed in the experiment through the maximum ice volume in the preceding glacial (Fig. 8). A large range of possible volume changes between glacial and interglacial conditions is observed for the LIG, which spans between 3.9 m SLE (for $\kappa = 0$) and 8.3 m SLE (for $\kappa = 20$

5   m a^{-1} K^{-1}). In the cases with largest κ values, the amount of ice lost entering the interglacial is larger than the present-day GrIS ice volume.

All the GrIS configurations simulated at the LIG ice minimum (Eemian) present a similar extension (Fig. 6 d-f). In all experiments, a large retreat is observed in the north (especially in northeast), where melting is sustained by the low accumulation, and in the southwest, where the ice discharge from the interior is enhanced by the presence of fast ice streams and, in some

10   areas, by the fact that the bedrock is below sea level. Although the position of the land-ice borders at the Eemian is not very sensitive to κ, the corresponding surface elevation fields show some differences depending on κ. For high values of κ, a lower ice elevation is simulated overall the GrIS (compare Fig. 6 d and f), tendency that is reflected in a slightly lower ice volume too (Fig. 5).

It is interesting to note that even when imposing a very high κ, the complete disappearance of the Greenland ice is not sim-

15   ulated. The GrIS is only partly deglaciated and all the ice core sites are still covered by ice (including the discussed ice core locations of Dye3 and NEEM). This behaviour is mainly controlled by the atmospheric temperatures and precipitations with which the model is forced, as the oceanic-driven retreat is limited by the land-based configuration observed in the interglacials. Figure 10 shows the evolution of the ice volume during the LIG for different values of the heat-flux coefficient κ. All volumes have been converted to SLE anomalies with respect to the present-day simulated by GRISLI-UCM in each specific experi-

20   ment. The amount of ice lost during the Eemian relative to the present day, which ranges between 2.8-3.3 m SLE, is within the uncertainty range of ice volumes suggested by some previous studies (e.g., 1.2-3.5 m SLE for Helsen et al. (2013), 0.4-4.4 m SLE for Robinson et al. (2011) and 0.4-3.8 m SLE for Stone et al. (2013)). Also, the timing at which the peak of deglaciation occurs, which spans between 122.5 and 121.5 ka BP in all the simulations, agrees with the timing proposed in many previous studies (Calov et al., 2015; Langebroek and Nisancioglu, 2016; Robinson et al., 2011; Stone et al., 2013; Yau et al., 2016).

3.4 Last Glacial Maximum

Although many uncertainties about the GrIS configuration during the last glacial period still exist, several estimates of the sea level contribution from the GrIS during the last deglaciation can be found in literature: 2.7 m SLE (Huybrechts, 2002), between 2 and 3 m SLE (Clark and Mix, 2002), 3.1 m SLE (Fleming and Lembeck, 2004), 4.1 m SLE (Simpson et al., 2009)

30   and 4.7 m SLE (Lecavalier et al., 2014). All of these estimates come from ice sheet models of different complexity, with their own dynamics and boundary conditions. Particularly the ice-sheet model of the most recent studies (Simpson et al., 2009; Lecavalier et al., 2014) is run in combination with a glacial isostatic adjustment and a Relative Sea Level (RSL) model and then constrained by past surface elevations derived from ice-core data, observations of RSL past changes and the present-day

GrIS configuration. These recent models do not solve the dynamics of the ice shelves and the grounding line migration is not simulated but parametrised. However, their estimates of the GrIS spatial extent and inferred ice volume can be considered as the most realistic reconstructions of the recent past glacial GrIS so far.

Figure 11 shows the evolution of the ice volume during the Holocene simulated by GRISLI-UCM for different values of κ.

5 Under constant oceanic conditions (grey band), the LGM ice excess with respect to the present simulated by our model ranges between -0.8 and 0.6 m SLE. The negative values correspond to a GrIS with less ice at the LGM than in the simulated present day, which is clearly unrealistic. The range of positive values (0-0.6 m SLE), however, also are well below previous LGM ice volume reconstructions found in the literature (grey points plotted at 21 ka BP). Thus even though paleoclimatic atmospheric temperatures and precipitations are able to force the GrIS to slightly grow during the glacials, the atmospheric forcing alone

10 is not able to make the GrIS expand as expected during the LGM. These inferences are confirmed in Fig. 12, where the LGM GrIS extent simulated by our model under constant oceanic forcing is shown (red line) and compared with that obtained by Lecavalier et al. (2014) (black line). Our simulation for $\kappa = 0$ suggests that during the LGM the GrIS would have remained almost land-based, limited to the above-sea-level land area, as also shown in Fig. 9 a. On the other hand, Lecavalier et al. (2014) reconstruct a GrIS extent as far as the continental shelf break in every direction, except in the northeast region where

15 the grounding line remains closer to the coast.

In contrast, the ice volume simulated by our model at the LGM when the oceanic forcing is active spans a large range of values, from 0.2 to 5.2 m SLE (Fig. 11). In this set of experiments, the GrIS reaches a LGM ice volume that is consistent with the literature for $\kappa = 1$ m a^{-1} K^{-1}, as the grounding line advances towards the continental shelf (Fig. 12). However, only with κ between 8 and 15 m a^{-1} K^{-1} does the model simulate a maximum ice volume of 4.5-4.7 m SLE, which is comparable to the

20 ranges given by Simpson et al. (2009) and Lecavalier et al. (2014).

The timing of the reconstructed deglaciation can also provide information for comparison. The maximum increase suggested by Simpson et al. (2009) (4.6 m SLE) and Lecavalier et al. (2014) (5.1 m SLE) occurs at 16.5 ka BP, while our simulations suggest a timing dependent on κ ranging from 18.8 to 10.4 ka BP for very low κ values (Fig. 11). The magnitudes of the oceanic sensitivity that best approximate the evolution of the GrIS before the Holocene are thus restricted to 10 m a^{-1} K^{-1}

25 (5.1 m SLE at 14.8 ka BP) and 15 m a^{-1} K^{-1} (5.3 m SLE at 13.7 ka BP). However some discrepancies between our results and theirs are still present. For $\kappa = 10$ m a^{-1} K^{-1} (at the LGM) the GrIS also extends to the continental shelf break in the northeast and the extension in small regions of the southwest, north-west and in the east slightly disagree with the grounding line position suggested by Lecavalier et al. (2014).

3.5 Present-day GrIS

30 Given that the topography of the present-day GrIS is one of the trustworthy measures used to assess the reliability of an ice-sheet model, we compare our present-day GrIS ice thickness and extent simulated for $\kappa = 10$ m a^{-1} K^{-1} to those estimated by Bamber et al. (2013) (Fig. 13). The choice of this particular κ value is based on the discussion above (Section 3.4) for the LGM and is supported by the good agreement between the simulated present-day ice volume and observations (Bamber et al., 2013) (Fig. 5). The two GrIS extents match reasonably. However, notable discrepancies are observed in some sectors. The

main differences are found in the northeast, where GRISLI-UCM predicts an extent more receded inland, and in the southwest, where our model is not able to make the GrIS retreat as expected. The ice loss in the north is a known problem that appears in many studies when simulating the GrIS during an interglacial (Stone et al., 2010; Born and Nisancioglu, 2012). In the interior, the difference in ice thickness is relatively low. However, the GrIS simulated by our model generally shows thicker ice along

5 the margins, a tendency that propagates inland. The only areas in which our simulated ice thickness is lower than that observed are located in the centre of the continent and in the very southeast corresponding to a mountainous region. However, the focus of our work is not to exactly reproduce the observed present-day GrIS ice volume at the end of the simulations, but rather to demonstrate the impact of the ocean on the advance and retreat of the whole GrIS throughout the past glacial cycles.

4   Discussion

10 Our model simulates the advance and retreat of the GrIS during the last two glacial cycles. The minimum ice volume distribution and the maximum ice volume loss are limited to a range constrained by the GrIS land-based configuration in warm periods and to the imposed glacial maximum extension at the continental shelf break, respectively. Since the interglacial GrIS is less exposed to oceanic variations, the minimum is constrained to a small range of possible values, while the maximum volume reached in cold periods is more sensitive to κ. During interglacials, the large ice mass loss observed for a high oceanic

15 sensitivity is closely related to the GrIS configuration in the previous glacial, which is totally marine-based at the margins and therefore more exposed to oceanic temperature variations (Fig. 6 c). As oceanic temperatures rise at the beginning of the deglaciation, basal melting rate increases too, thinning the ice shelves at the boundaries, enhancing ice mass loss at the marine-terminating margins and triggering grounding line retreat. The effects of this ocean-driven retreat are not locally confined but are propagated inland through a dynamic response of the grounded ice sheet. The loss of ice at the GrIS margins triggers the

20 advection of ice from the interior, further increasing the ice discharge into the ocean. As the thickness of the inner ice decreases, the elevation-melt feedback is activated. At a given stage of the deglaciation, when the whole ice sheet starts to be land-based, this atmosphere-driven retreat becomes the sole driver of ice mass loss.

As discussed in Sections 3.4 and 3.5, the oceanic forcing that seems to best reconstruct the past (LGM) and the present GrIS is achieved for a heat-flux coefficient of $10 \, \mathrm{m \, a^{-1} \, K^{-1}}$. However we have to bear in mind that in these tests only a limited range

25 of reference submarine melting rates has been investigated, having explored only a portion of the phase-space in the system of model parameters (Table 1).

We are aware that the melting rate depends on many regional factors such as the temperature of the ocean at the ice-shelf margin, the shape of the ice-shelf cavity and the depth of the grounding line. However, we are considering the same order of magnitude of melt rates as is proposed in the literature, although for the AIS case, which spans values from negative to above

30 $40 \, \mathrm{m \, a^{-1}}$ in some very active regions (Rignot and Jacobs, 2002). Moreover, in support of this evidence, similar basal melting rates have been found recently in some GrIS ice tongues (Wilson et al., 2017).

The basal melting equation at the grounding line also depends on ΔT_{ocn}, which in turn is function of the climatic index α and the oceanic temperature anomaly $T_{\mathrm{LGM,ocn}} - T_{\mathrm{PD, ocn}}$. The latter field has been prescribed to a spatially constant value of $-3K$

and it impacts the oceanic sensitivity through the heat-flux coefficient κ. It is thus clear that the same results obtained in this work would have been obtained by keeping constant κ and by examining the influence of different levels of the ΔT_{ocn} in the GrIS past evolution. Considering a spatially constant SST anomaly represents an idealized simplification of the oceanic forcing. However, taking into account spatially variable (horizontally and vertically) past oceanic temperatures, the main results

5 obtained in this work would not change except for the optimal value of the oceanic sensitivity parameter κ.

Our results may well be model-dependent, and some model limitations should be noted. The simulated ice volume at the present day is overestimated for all investigated values of κ (Fig. 8). This fact suggests that our model has a tendency to overestimate the ice thickness of the GrIS, especially in the marginal zones of the domain, a well known phenomenon (Calov et al., 2015). These discrepancies are partly linked to the relatively low applied model resolution (20 x 20 km), which limits the accuracy in

10 estimating the margins especially along the fjords, and partly due to the boundary conditions applied to the ice-sheet model, such as the basal sliding. The coarse model resolution prevents the model from resolving fine-scale physical processes at the marine-terminating outlet glaciers that end in narrow fjords, although they are considered as the primary sources of ice discharge today due to oceanic changes. Especially when, as in our case, the submarine melt goes abruptly to a high value at the grounding line, the implementation of a sub-grid scale parametrisation would allow the small processes at the fjords to be

15 accurately solved (Calov et al., 2015; Favier et al., 2016; Gladstone et al., 2017). However, as the main objective of the paper is to analyse the dynamic evolution of the whole GrIS over glacial cycles, the lack of a sub-grid resolution at the grounding line is here not as relevant an issue as for studies focusing on shorter time scales.

The parametrisation used for the submarine melting rate at the GrIS marine margins is implemented in such a way that the melting at the grounding line (Eq. 10) is higher ~~that~~ the one set below the ice shelves (Eq. 11). This approach is supported by

20 sub-shelf melting rate estimates (Dutrieux et al., 2013; Reese et al., 2017; Rignot and Jacobs, 2002; Wilson et al., 2017). However recent work shows the necessity to make the basal melting decrease smoothly to zero when approaching the grounding line from the ice shelf to avoid resolution-dependent performances (Gladstone et al., 2017). That approach can be obtained for example by considering the submarine melt to be dependent on the water-column thickness beneath the ice shelf. Following these assumptions, a sub-grid treatment of the small processes taking place at the grounding line will be added in our model in

25 the future. This will provide a more realistic description of grounding-line processes such as the enhanced submarine melting as well as the basal drag at the margin of fast grounded ice, and reduce the model dependency of the results, in general.

5 Conclusions

Here we assessed the impact of paleo oceanic temperature variations on the evolution of the GrIS on a glacial/interglacial time scale. By using a three-dimensional hybrid ice-sheet/ice-shelf model including a parametrisation of the basal melting

30 rate at the GrIS marine margins, the model simulates the evolution of the whole ice sheet under variable oceanic conditions. Firstly, the magnitude of the oceanic forcing applied at the ice-ocean interface triggers and drives the grounding line advance (through water freezing) and retreat (through ice melting). Second, it induces a dynamic adjustment of the grounded ice sheet, determining the amount of ice grown (lost) during the cold (warm) stages. Although the GrIS evolution is a result of the

atmospheric and oceanic forcings operating together, we have shown that the atmospheric forcing alone is not capable of accounting for the expected evolution of the GrIS. Not only must the oceanic forcing be activated, but it must be strong enough to reproduce a reliable GrIS evolution throughout the glacial cycles. Thus, changes in oceanic conditions are a primary factor driving the evolution of the whole GrIS, suggesting that the oceanic component should be included as an active forcing in paleo

5   ice sheet models.

Code and data availability.   The GRISLI-UCM code and the analysed data are available from the authors upon request.

Author contributions.   I. Tabone carried out the simulations, analysed the results and wrote the manuscript. All other authors contributed to design the simulations, to analyse the results and to write the paper.

Competing interests.   The authors declare no competing interests related to this work.

10   *Acknowledgements.*   We would like to thank C. Ritz for providing the former Grisli. This work was funded by the Spanish Ministry of Science and Innovation under the project MOCCA (Modelling Abrupt Climate Change, Grant no. CGL2014-59384-R). A. Robinson is funded by the Marie Curie Horizon2020 project CONCLIMA (Grant no. 703251). All of these simulations were performed in EOLO, the HPC of Climate Change of the International Campus of Excellence of Moncloa, funded by MECD and MICINN.

References

Alley, R. B., Anandakrishnan, S., Christianson, K., Horgan, H. J., Muto, A., Parizek, B. R., Pollard, D., and Walker, R. T.: Oceanic forcing of Ice-Sheet retreat: West Antarctica and more, Annu. Rev. Earth Planet. Sci., 43, 207–231, https://doi.org/10.1146/annurev-earth-060614-105344, 2015.

5 Alvarez-Solas, J., Montoya, M., Ritz, C., Ramstein, G., Charbit, S., Dumas, C., Nisancioglu, K., Dokken, T., and Ganopolski, A.: Millennial-scale oscillations in the Southern Ocean in response to atmospheric CO2 increase, Global Planet. Change, 76, 128–136, https://doi.org/10.5194/cp-7-1297-2011, 2010.

Alvarez-Solas, J., Montoya, M., Ritz, C., Ramstein, G., Charbit, S., Dumas, C., Nisancioglu, K., Dokken, T., and Ganopolski, A.: Heinrich event 1: an example of dynamical ice-sheet reaction to oceanic changes, Clim. Past, 7, 1297–1306, https://doi.org/10.5194/cp-7-1297-2011, 2011.

10 Alvarez-Solas, J., Robinson, A., Montoya, M., and Ritz, C.: Iceberg discharges of the last glacial period driven by oceanic circulation changes, PNAS, 110, 41, 16 350–16 354, https://doi.org/10.1073/pnas.1306622110, 2013.

Bamber, J. L., Griggs, J. A., Hurkmans, R. T. W. L., Dowdeswell, J. A., Gogineni, S. P., Howat, I., Mouginot, J., Paden, J., Palmer, S., Rignot, E., and Steinhage, D.: A new bed elevation dataset for Greenland, The Cryosphere, 7, 499–510, https://doi.org/10.5194/tc-7-499-2013, 15 2013.

Banderas, R., Alvarez-Solas, J., Robinson, A., and Montoya, M.: A new approach for simulating the paleo evolution of the Northern Hemisphere ice sheets, Geoscientific Model Development Discussions, 2017, 1–24, https://doi.org/10.5194/gmd-2017-158, 2017.

Barker, S., Knorr, G., Edwards, R. L., Parrenin, F., Putnam, A. E., Skinner, L. C., Wolff, E., and Ziegler, M.: 800,000 years of abrupt climate variability, Science, 334, 347–351, https://doi.org/10.1126/science.1203580, 2011.

20 Beckmann, A. and Goosse, H.: A parameterization of ice shelf-ocean interaction for climate models, Ocean Model., 5, 157–170, https://doi.org/10.1016/S1463-5003(02)00019-7, 2003.

Bindschadler, R. A., Nowicki, S., Abe-Ouchi, A., Aschwanden, A., Choi, H., Fastook, J., Granzow, G., Greve, R., Gutowski, G., Herzfeld, U., Jackson, C., Johnson, J., Khroulev, C., Levermann, A., Lipscomb, W. H., Martin, M. A., Morlighem, M., Parizek, B. R., Pollard, D., Price, S. F., Ren, D., Saito, F., Sato, T., Seddik, H., Seroussi, H., Takahashi, K., Walker, R., and Wang, W. L.: Ice sheet model sensitivity to 25 environmental forcing and their use in projecting future sea level, J. Glaciol., 59, 195–224, https://doi.org/10.3189/2013JoG12J125, 2013.

Born, A. and Nisancioglu, K. H.: Melting of Northern Greenland during the last interglaciation, The Cryosphere, 6, 1239–1250, https://doi.org/10.5194/tc-6-1239-2012, 2012.

Box, J. E., Yang, L., Bromwich, D. H., and Bai, L.-S.: Greenland ice sheet surface air temperature variability: 1840-2007, Journal of Climate, 22 (14), 4029–4049, https://doi.org/10.1175/2009JCLI2816.1, 2009.

30 Bueler, E. and Brown, J.: Shallow shelf approximation as a "sliding law´´ in a thermomechanically coupled ice sheet model, J. Geophys. Res., 114, F03 008, https://doi.org/10.1029/2008JF001179, 2009.

Calov, R., Robinson, A., Perrette, M., and Ganopolski, A.: Simulating the Greenland ice sheet under present-day and palaeo constraints including a new discharge parameterization, The Cryosphere, 9, 179–196, https://doi.org/10.5194/tc-9-179-2015, 2015.

Church, J., Clark, P., Cazenave, A., Gregory, J., Jevrejeva, S., Levermann, A., Merrifield, M., Milne, G., Nerem, R., Nunn, P., Payne, A., 35 Pfeffer, W., D., S., and Unnikrishnan, A.: Sea Level Change, Climate Change 2013: The Physical Science Basis. Contribution of Working Group I to the Fifth Assessment Report of the Intergovernmental Panel on Climate Change, 2013.

Clark, P. U. and Mix, A. C.: Ice sheets and sea level of the Last Glacial Maximum, Quat. Sci. Rev., 21(1), 1–7, 2002.

Clark, P. U., Church, J. A., Gregory, J. M., and Payne, A. J.: Recent progress in understanding and projecting regional and global mean sea level change, Current Climate Change Reports, 1, 224–246, 2015.

Cook, A. J., Holland, P. R., Meredith, M. P., Murray, T., Luckman, A., and Vaughan, D. G.: Ocean forcing of glacier retreat in the western Antarctic Peninsula, Science, 353(6296), 283–286, https://doi.org/10.1126/science.aae0017, 2016.

5 DeConto, R. M. and Pollard, D.: Contribution of Antarctica to past and future sea-level rise, Nature, 531, 591–597, https://doi.org/10.1038/nature17145, 2016.

Dutrieux, P., Vaughan, D. G., Corr, H. F., Jenkins, A., Holland, P. R., Joughin, I., and Fleming, A.: Pine Island glacier ice shelf melt distributed at kilometre scales, The Cryosphere, 7, 1543–1555, https://doi.org/10.5194/tc-7-1543-2013, 2013.

Enderlin, E. M. and Howat, I. M.: Submarine melt rate estimates for floating termini of Greenland outlet glaciers (2000-2010), Journal of
10 Glaciology, 59(213), 67–75, https://doi.org/10.3189/2013JoG12J049, 2013.

Favier, L., Durand, G., Cornford, S. L., Gudmundsson, G. H., Gagliardini, O., Gillet-Chaulet, F., Zwinger, T., Payne, A., and Le Brocq, A. M.: Retreat of Pine Island Glacier controlled by marine ice-sheet instability, Nature Climate Change, 4, 117–121, https://doi.org/10.1038/NCLIMATE2094, 2014.

Favier, L., Pattyn, F., Berger, S., and Drews, R.: Dynamic influence of pinning points on marine ice-sheet stability: a numerical study in
15 Dronning Maud Land, East Antarctica, The Cryosphere, 10, 2623–2635, https://doi.org/10.5194/tc-10-2623-2016, 2016.

Fettweis, X., Franco, B., Tedesco, M., Van Angelen, J., Lenaerts, J., Van den Broeke, M., and Gallée, H.: Estimating Greenland ice sheet surface mass balance contribution to future sea level rise using the regional atmospheric climate model MAR, The Cryosphere, 7, 469–489, https://doi.org/10.5194/tc-7-469-2013, 2013.

Fleming, K. and Lembeck, K.: Constraints on the Greenland Ice Sheet since the Last Glacial Maximum from sea-level observations and
20 glacial-rebound models, Quat. Sci. Rev., 23(9), 1053–1077, https://doi.org/10.1016/j.quascirev.2003.11.001, 2004.

Fried, M., Catania, G., Bartholomaus, T., Duncan, D., Davis, M., Stearns, L., Nash, J., Shroyer, E., and Sutherland, D.: Distributed subglacial discharge drives significant submarine melt at a Greenland tidewater glacier, Geophys. Res. Lett., 42(21), 9328–9336, https://doi.org/10.1002/2015GL065806, 2015.

Fürst, J. J., Goelzer, H., and Huybrechts, P.: Effect of higher-order stress gradients on the centennial mass evolution of the Greenland ice
25 sheet, The Cryosphere, 7, 183–199, https://doi.org/10.5194/tc-7-183-2013, 2013.

Fürst, J. J., Goelzer, H., and Huybrechts, P.: Ice-dynamic projections of the Greenland ice sheet in response to atmospheric and oceanic warming, The Cryosphere, 9, 1039–1062, https://doi.org/10.5194/tc-9-1039-2015, 2015.

Gladstone, R. M., Warner, R. C., Galton-Fenzi, B. K., Gagliardini, O., Zwinger, T., and Greve, R.: Marine ice sheet model performance depends on basal sliding physics and sub-shelf melting, The Cryosphere, 2017, 319–329, https://doi.org/10.5194/tc-11-319-2017, 2017.

30 Golledge, N. R., Fogwill, C. J., Mackintosh, A. N., and Buckley, K. M.: Dynamics of the last glacial maximum Antarctic ice-sheet and its response to ocean forcing, PNAS, 109(40), 16 052–16 056, https://doi.org/10.1073/pnas.1205385109, 2012.

Hall, D. K., Williams, R. S., Luthcke, S. B., and Digirolamo, N. E.: Greenland ice sheet surface temperature, melt and mass loss: 2000-06, Journal of Glaciology, 54 (184), 81–93, 2008.

Hanna, E., Navarro, F. J., Pattyn, F., Domingues, C. M., Fettweis, X., Ivins, E. R., Nicholls, R. J., Ritz, C., Smith, B., Tulaczyk, S., White-
35 house, P. L., and Zwally, H. J.: Ice-sheet mass balance and climate change, Nature, 498, 51–59, https://doi.org/10.1038/nature12238, 2013.

Helsen, M., Van De Berg, W., Van De Wal, R., Van Den Broeke, M., and Oerlemans, J.: Coupled regional climate-ice-sheet simulation shows limited Greenland ice loss during the Eemian, Clim. Past, 9(4), 1773, https://doi.org/10.5194/cp-9-1773-2013, 2013.

Hogg, A. E. and Gudmundsson, G. H.: Impacts of the Larsen-C Ice Shelf calving event, Nat. Clim. Change, 7, 540–542, https://doi.org/10.1038/nclimate3359, 2017.

Holland, D. M., Thomas, R. H., De Young, B., Ribergaard, M. H., and Lyberth, B.: Acceleration of Jakobshavn Isbræ triggered by warm subsurface ocean waters, Nat. Geosci., 1, 659–664, https://doi.org/10.1038/ngeo316, 2008a.

5 Holland, P., Brisbourne, A., Corr, H., Mcgrath, D., Purdon, K., Paden, J., Fricker, H., Paolo, F., and Fleming, A.: Oceanic and atmospheric forcing of Larsen C Ice-Shelf thinning, The Cryosphere, 9, 1005–1024, https://doi.org/10.5194/tc-9-1005-2015, 2015.

Holland, P. R., Jenkins, A., and Holland, D. M.: The response of ice shelf basal melting to variations in ocean temperature, J. Clim., 21, 2558–2572, https://doi.org/10.1175/2007JCLI1909.1, 2008b.

Howat, I. M., Joughin, I., Tulaczyk, S., and Gogineni, S.: Rapid retreat and acceleration of Helheim Glacier, east Greenland, Geophys. Res.
10 Lett., 32, L22 502, https://doi.org/10.1029/2005GL024737, 2005.

Howat, I. M., Joughin, I., and Scambos, T. A.: Rapid changes in ice discharge from Greenland outlet glaciers, Science, 315, 1559–1561, https://doi.org/10.1126/science.1138478, 2007.

Huybrechts, P.: Sea-level changes at the LGM from ice-dynamic reconstructions of the Greenland and Antarctic ice sheets during the glacial cycles, Quat. Sci. Rev., 21, 203–231, https://doi.org/10.1016/S0277-3791(01)00082-8, 2002.

15 Jansen, D., Luckman, A. J., Cook, A., Bevan, S., Kulessa, B., Hubbard, B., and Holland, P.: Brief Communication: Newly developing rift in Larsen C Ice Shelf presents significant risk to stability, The Cryosphere, 9, 1223–1227, https://doi.org/10.5194/tc-9-1223-2015, 2015.

Jenkins, A.: Convection-driven melting near the grounding line of ice shelves and tidewater glaciers, J. Phys. Oceanogr., 41, 2279–2294, https://doi.org/10.1175/JPO-D-11-03.1, 2011.

Joughin, I., Smith, B. E., Howat, I. M., Floricioiu, D., Alley, R. B., Truffer, M., and Fahnestock, M.: Seasonal to decadal scale varia-
20 tions in the surface velocity of Jakobshavn Isbræ, Greenland: Observation and model-based analysis, J. Geophys. Res., 117, F02 030, https://doi.org/10.1029/2011JF002110, 2012.

Joughin, I., Smith, B. E., and Medley, B.: Marine ice sheet collapse potentially under way for the Thwaites Glacier Basin, West Antarctica, Science, 344, 735–738, https://doi.org/10.1126/science.1249055, 2014a.

Joughin, I., Smith, B. E., and Medley, B.: Marine ice sheet collapse potentially under way for the Thwaites Glacier Basin, West Antarctica,
25 Science, 344(6185), 735–738, https://doi.org/10.1126/science.1249055, 2014b.

Kindler, P., Guillevic, M., Baumgartner, M., Schwander, J., Landais, A., and Leuenberger, M.: Temperature reconstruction from 10 to 120 kyr b2k from the NGRIP ice core, Clim. Past, 10, 887–902, https://doi.org/10.5194/cp-10-887-2014, 2014.

Langebroek, P. M. and Nisancioglu, K. H.: Moderate Greenland ice sheet melt during the last interglacial constrained by present-day obser- vations and paleo ice core reconstructions, The Cryosphere Discuss., pp. 1–35, https://doi.org/10.5194/tc-2016-15, 2016.

30 Le Meur, E. and Huybrechts, P.: A comparison of different ways of dealing with isostasy: examples from modeling the Antarctic ice sheet during the last glacial cycle, Annals of Glaciology, 23, 309–317, 1996.

Lecavalier, B. S., Milne, G. A., Simpson, M. J., Wake, L., Huybrechts, P., Tarasov, L., Kjeldsen, K. K., Funder, S., Long, A. J., Woodroffe, S., Dykei, A. S., and Larsen, N. K.: A model of Greenland ice sheet deglaciation constrained by observations of relative sea level and ice extent, Quat. Science Rev., 102, 54–84, https://doi.org/10.1016/j.quascirev.2014.07.018, 2014.

35 MARGO, P. m.: Constraints on the magnitude and patterns of ocean cooling at the Last Glacial Maximum, Nat. Geosci., 2, 127–132, https://doi.org/10.1038/ngeo411, 2009.

Montoya, M. and Levermann, A.: Surface wind-stress threshold for glacial Atlantic overturning, Geophys. Res. Lett., 35, L03 608, https://doi.org/10.1029/2007GL032560, 2008.

Morlighem, M., Bondzio, J., Seroussi, H., Rignot, E., Larour, E., Humbert, A., and Rebuffi, S.: Modeling of Store Gletscher's calving dynamics, West Greenland, in response to ocean thermal forcing, Geophys. Res. Lett., 43, 6, https://doi.org/10.1002/2016GL067695, 2016.

Motyka, R. J., Truffer, M., Fahnestock, M., Mortensen, J., Rysgaard, S., and Howat, I.: Submarine melting of the 1985 Jakobshavn Isbræ
5   floating tongue and the triggering of the current retreat, J. Geophys. Res., 116, F01 007, https://doi.org/10.1029/2009JF001632, 2011.

NEEM: Eemian interglacial reconstructed from a Greenland folded ice core, Nature, 493, 489–494, https://doi.org/10.1038/nature11789, 2013.

Nick, F. M., Vieli, A., Howat, I. M., and Joughin, I.: Large-scale changes in Greenland outlet glacier dynamics triggered at the terminus, Nat. Geosci., 2, 110–114, https://doi.org/10.1038/ngeo394, 2009.

10 Nowicki, S., Bindschadler, R. A., Abe-Ouchi, A., Aschwanden, A., Bueler, E., Choi, H., Fastook, J., Granzow, G., Greve, R., and Gutowski, G.: Large-scale changes in Greenland outlet glacier dynamics triggered at the terminus, J. Geophys. Res.: Earth Surface, 118, 1025–1044, https://doi.org/10.1002/jgrf.20076, 2013.

Pattyn, F.: Sea-level response to melting of Antarctic ice shelves on multi-centennial time scales with the fast Elementary Thermomechanical Ice Sheet model (f.ETISh v1.0), The Cryosphere, 8, 1–52, https://doi.org/10.5194/tc-2017-8, 2017.

15 Philippon, G., Ramstein, G., Charbit, S., Kageyama, M., Ritz, C., and Dumas, C.: Evolution of the Antarctic ice sheet throughout the last deglaciation: A study with a new coupled climate—north and south hemisphere ice sheet model, Earth Planet. Sc. Lett, 248, 750–758, https://doi.org/10.1016/j.epsl.2006.06.017, 2006.

Pollard, D. and DeConto, R. M.: Description of a hybrid ice sheet-shelf model, and application to Antarctica, Geosci. Model Dev., 5, 1273–1295, https://doi.org/10.5194/gmd-5-1273-2012, 2012.

20 Pritchard, H. D., Ligtenberg, S. R. M., Fricker, H. A., Vaughan, D. G., Van den Broeke, M. R., and Padman, L.: Antarctic ice-sheet loss driven by basal melting of ice shelves, Nature, 484, 502–505, https://doi.org/10.1038/nature10968, 2012.

Quiquet, A., Punge, H., Ritz, C., Fettweis, X., Kageyama, M., Krinner, G., Salas y Mélia, D., and Sjolte, J.: Sensitivity of a Greenland ice sheet model to atmospheric forcing fields, The Cryosphere, 6, 999–1018, https://doi.org/10.5194/tc-6-999-2012, 2012.

Quiquet, A., Ritz, C., Punge, H. J., and Salas y Mélia, D.: Greenland Ice Sheet contribution to sea level rise during the last geoscientific
25 interglacial period: a modelling study driven and Instrumentation constrained by methods and ice core data, Clim. Past, 9, 353–366, https://doi.org/10.5194/cp-9-353-2013, 2013.

Reeh, N.: Parameterization of melt rate and surface temperature on the Greenland ice sheet, Polarforschung, 59, 113–128, 1989.

Reese, R., Albrecht, T., Mengel, M., Asay-Davis, X., and Winkelmann, R.: Antarctic sub-shelf melt rates via PICO, The Cryosphere Discuss., pp. 1–24, https://doi.org/10.5194/tc-2017-70, 2017.

30 Rignot, E. and Jacobs, S. S.: Rapid bottom melting widespread near Antarctic Ice Sheet grounding lines, Science, 296, 2020–2023, https://doi.org/10.1126/science.1070942, 2002.

Rignot, E. and Kanagaratnam, P.: Changes in the velocity structure of the Greenland Ice Sheet, Science, 311(5763), 986–990, https://doi.org/10.1126/science.1121381, 2006.

Rignot, E., Casassa, G., Gogineni, P., Krabill, W., Rivera, A. u., and Thomas, R.: Accelerated ice discharge from the Antarctic Peninsula
35 following the collapse of Larsen B ice shelf, Geophys. Res. Lett., 31, L18 401, https://doi.org/10.1029/2004GL020697, 2004.

Rignot, E., Koppes, M., and Velicogna, I.: Rapid submarine melting of the calving faces of West Greenland glaciers, Nat. Geosci., 3, 187–191, https://doi.org/10.1038/ngeo765, 2010.

Rignot, E., Velicogna, I., Van den Broeke, M. R., Monaghan, A., and Lenaerts, J. T. M.: Acceleration of the contribution of the Greenland and Antarctic ice sheets to sea level rise, Geophys. Res. Lett., 38, L05 503, https://doi.org/10.1029/2011GL046583, 2011.

Rignot, E., Jacobs, S., Mouginot, J., and Scheuchl, B.: Ice-shelf melting around Antarctica, Science, 341(6143), 266–270, https://doi.org/10.1126/science.1235798, 2013.

5 Rignot, E., Mouginot, J., Morlighem, M., Seroussi, H., and Scheuchl, B.: Widespread, rapid grounding line retreat of Pine Island, Thwaites, Smith, and Kohler glaciers, West Antarctica, from 1992 to 2011, Geophys. Res. Lett., 41, 10, 3502–3509, https://doi.org/10.1002/2014GL060140, 2014.

Rignot, E., Xu, Y., Menemenlis, D., Mouginot, J., Scheuchl, B., Li, X., Morlighem, M., Seroussi, H., Broeke, M. v., Fenty, I., Cai, C., An, L., and de Fleurian, B.: Modeling of ocean-induced ice melt rates of five west Greenland glaciers over the past two decades, Geophys. Res. Lett., 43, 6374–6382, https://doi.org/10.1002/2016GL068784, 2016.

Ritz, C., Rommelaere, V., and Dumas, C.: Modeling the evolution of Antarctic Ice Sheet over the last 420,000 years. Implications for altitude changes in the Vostok region, J. Geophys. Res., 106(D23), 31 943–31 964, https://doi.org/10.1029/2001JD900232, 2001.

Robinson, A. and Goelzer, H.: The importance of insolation changes for paleo ice sheet modeling, The Cryosphere, 8, 1419–1428, https://doi.org/10.5194/tc-8-1419-2014, 2014.

15 Robinson, A., Calov, R., and Ganopolski, A.: Greenland ice sheet model parameters constrained using simulations of the Eemian Interglacial, Clim. Past, 7, 381–396, https://doi.org/10.5194/cp-7-381-2011, 2011.

Sasgen, I., van den Broeke, M., Bamber, J. L., Rignot, E., Sørensen, L. S., Wouters, B., Martinec, Z., Velicogna, I., and Simonsen, S. B.: Timing and origin of recent regional ice-mass loss in Greenland, Earth Planet. Sc. Lett., 333-334, 293–303, https://doi.org/10.1016/j.epsl.2012.03.033, 2012.

20 Sciascia, R., Straneo, F., Cenedese, C., and Heimbach, P.: Seasonal variability of submarine melt rate and circulation in an East Greenland fjord, J. Geophys. Res. Oceans, 118, 2492–2506, https://doi.org/10.1002/jgrc.20142, 2013.

Shapiro, N. M. and Ritzwoller, M. H.: Inferring surface heat flux distributions guided by a global seismic model: particular application to Antarctica, Earth Planet. Sc. Lett., 223, 213–224, https://doi.org/10.1016/j.epsl.2004.04.011, 2004.

Shepherd, A., Wingham, D., and Rignot, E.: Warm ocean is eroding West Antarctic ice sheet, Geophys. Res. Lett., 31, L23 402, https://doi.org/10.1029/2004GL021106, 2004.

Shepherd, A., Ivins, E. R., Geruo, A., Barletta, V. R., Bentley, M. J., Bettadpur, S., Briggs, K. H., Bromwich, D. H., Forsberg, R., Galin, N., Horwath, M., Jacobs, S., Joughin, I., King, M. A., Lenaerts, J. T. M., Li, J., Ligtenberg, S. R. M., Luckman, A., Luthcke, S. B., McMillan, M., Meister, R., Milne, G., Mouginot, J., Muir, A., Nicolas, J. P., Paden, J., Payne, A. J., Pritchard, H., Rignot, E., Rott, H., Sandberg Sorensen, L., Scambos, T. A., Scheuchl, B., Schrama, E. J. O., Smith, B., Sundal, A. V., van Angelen, J. H., van de Berg, W. J.,

30 van den Broeke, M. R., Vaughan, D. G., Velicogna, I., Wahr, J., Whitehouse, P. L., Wingham, D. J., Yi, D., Young, D., and Zwally, H. J.: A reconciled estimate of ice sheet mass balance, Science, 338, 1183–1189, https://doi.org/10.1126/science.1228102, 2012.

Simpson, M. J. R., Milne, G. A., Huybrechts, P., and Long, A. J.: Calibrating a glaciological model of the Greenland ice sheet from the Last Glacial Maximum to present-day using fieldobservations of relative sea level and ice extent, Quat. Science Rev., 28(17), 1631–1657, https://doi.org/10.1016/j.quascirev.2009.03.004, 2009.

35 Stearns, L. A. and Hamilton, G. S.: Rapid volume loss from two East Greenland outlet glaciers quantified using repeat stereo satellite imagery, Geophys. Res. Lett., 34, L05 503, https://doi.org/10.1029/2006GL028982, 2007.

Stone, E., Lunt, D., Annan, J., and Hargreaves, J.: Quantification of the Greenland ice sheet contribution to Last Interglacial sea level rise, Clim. Past, 9, 621–639, https://doi.org/10.5194/cp-9-621-2013, 2013.

Stone, E. J., Lunt, D. J., Rutt, I. C., and Hanna, E.: Investigating the sensitivity of numerical model simulations of the modern state of the Greenland ice-sheet and its future response to climate change, The Cryosphere, 4, 397–417, https://doi.org/10.5194/tc-4-397-2010, 2010.

Straneo, F. and Heimbach, P.: North Atlantic warming and the retreat of Greenland's outlet glaciers, Nature, 504, 36–43, https://doi.org/10.1038/nature12854, 2013.

5 Straneo, F., Hamilton, G. S., Sutherland, D. A., Stearns, L. A., Davidson, F., Hammill, M. O., Stenson, G. B., and Rosing-Asvid, A.: Rapid circulation of warm subtropical waters in a major glacial fjord in East Greenland, Nat. Geosci., 3, 182–186, https://doi.org/10.1038/ngeo764, 2010.

Straneo, F., Sutherland, D. A., Holland, D., Gladish, C., Hamilton, G. S., Johnson, H. L., Rignot, E., Xu, Y., and Koppes, M.: Characteristics of ocean waters reaching Greenland's glaciers, Ann. Glaciol., 53(60), 202–210, https://doi.org/10.3189/2012AoG60A059, 2012.

10 Straneo, F., Hamilton, G. S., Stearns, L. A., and Sutherland, D. A.: Connecting the Greenland Ice Sheet and the ocean: a case study of Helheim Glacier and Sermilik Fjord, Oceanography, 29 (4), 22–33, https://doi.org/10.5670/oceanog.2016.97, 2016.

Sutherland, D. A. and Straneo, F.: Estimating ocean heat transports and submarine melt rates in Sermilik Fjord, Greenland, using lowered acoustic Doppler current profiler (LADCP) velocity profiles, Ann. Glaciol., 53(60), 50–58, https://doi.org/10.3189/2012AoG60A050, 2012.

15 Tarasov, L. and Peltier, R. W.: Greenland glacial history and local geodynamic consequences, Geophys. J. Int., 150, 198–229, 2002.

Tedesco, M., Doherty, S., Fettweis, X., Alexander, P., Jeyaratnam, J., and Stroeve, J.: The darkening of the Greenland ice sheet: trends, drivers, and projections (1981-2100), The Cryosphere, 10, 477–496, https://doi.org/10.5194/tc-10-477-2016, 2016.

van den Broeke, M. R., Enderlin, E. M., Howat, I. M., and Noël, B. P. Y.: On the recent contribution of the Greenland ice sheet to sea level change, The Cryosphere, 10, 1933–1946, https://doi.org/10.5194/tc-2016-123, 2016.

20 Vieli, A. and Nick, F. M.: Understanding and modelling rapid dynamic changes of tidewater outlet glaciers: issues and implications, Surveys in geophysics, 32, 437–458, https://doi.org/10.1007/s10712-011-9132-4, 2011.

Vinther, B. M., Buchardt, S. L., Clausen, H. B., Dahl-Jensen, D., Johnsen, S. J., Fisher, D., Koerner, R., Raynaud, D., Lipenkov, V., Andersen, K., et al.: Holocene thinning of the Greenland ice sheet, Nature, 461, 385–388, https://doi.org/10.1038/nature08355, 2009.

Wilson, N., Straneo, F., and Heimbach, P.: Submarine melt rates and mass balance for Greenland's remaining ice tongues, The Cryosphere Discuss., pp. 1–17, https://doi.org/10.5194/tc-2017-99, 2017.

25 Wouters, B., Martin-Español, A., Helm, V., Flament, T., van Wessem, J., Ligtenberg, S., van den Broeke, M., and Bamber, J.: Dynamic thinning of glaciers on the Southern Antarctic Peninsula, Science, 348, 899–903, https://doi.org/10.1126/science.aaa5727, 2015.

Xu, Y., Rignot, E., Menemenlis, D., and Koppes, M.: Numerical experiments on subaqueous melting of Greenland tidewater glaciers in response to ocean warming and enhanced subglacial discharge, Annals of Glaciology, 53, 229–234, https://doi.org/10.3189/2012AoG60A139, 2012.

30 Xu, Y., Rignot, E., Fenty, I., Menemenlis, D., and Flexas, M.: Subaqueous melting of Store Glacier, west Greenland from three-dimensional, high-resolution numerical modeling and ocean observations, Geophys. Res. Lett., 40, 4648–4653, https://doi.org/10.1002/grl.50825, 2013.

Yau, A. M., Bender, M. L., Robinson, A., and Brook, E. J.: Reconstructing the last interglacial at Summit, Greenland: Insights from GISP2, PNAS, 113(35), 9710–9715, https://doi.org/10.1073/pnas.1524766113, 2016.

35 Yi, S., Sun, W., Heki, K., and Qian, A.: An increase in the rate of global mean sea level rise since 2010, Geophys. Res. Lett., 42, 3998–4006, https://doi.org/10.1002/2015GL063902, 2015.

Zwally, H. J., Jun, L. I., Brenner, A. C., Beckley, M., Cornejo, H. G., DiMarzio, J., Giovinetto, M. B., Neumann, T. A., Robbins, J., Saba, J. L., Yi, D., and Wang, W.: Greenland ice sheet mass balance: distribution of increased mass loss with climate warming; 2003–07 versus 1992–2002, J. Glaciol., 57(201), 88–102, https://doi.org/10.3189/002214311795306682, 2011.

Table 1. Summary of all the parameter values used to perturb the basal melting rate equation (Eq. 10) in each sensitivity test.

Sensitivity to	Perturbed parameters	Units	Values
Reference submarine melting B_{ref}	B_{ref}	$\mathrm{m\,a^{-1}}$	0, 0.2, 0.5, 1, 3, 5, 8, 10, 20, 30, 40
	κ	$\mathrm{m\,a^{-1}\,K^{-1}}$	0
Heat-flux coefficient κ	B_{ref}	$\mathrm{m\,a^{-1}}$	0, 0.2, 0.5, 1, 3, 5, 8, 10, 20, 30, 40
	κ	$\mathrm{m\,a^{-1}\,K^{-1}}$	0, 0.2, 0.5, 1, 2, 3, 5, 8, 10, 15, 20
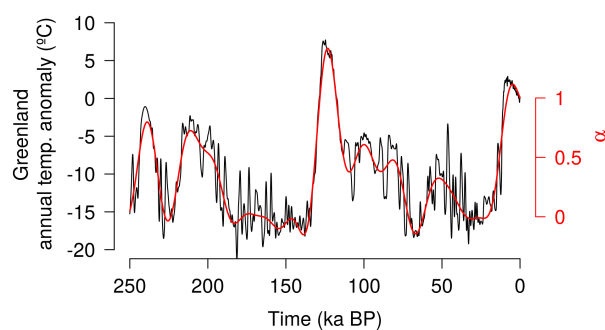
Figure 1. The 250 ka Greenland annual temperature anomaly signal built through a multi-proxy approach based on the reconstruction by Vinther et al. (2009) from 11.7 ka BP to present, the NGRIP reconstruction (Kindler et al., 2014) for 115-11.7 ka BP, the NEEM reconstruction (NEEM, 2013) for 135-115 ka BP and a synthetic temperature anomaly time series for the time period 250-135 ka BP following Barker et al. (2011) (black line). The red line shows the filtered and normalized climatic index α used to correct the present-day climatological fields when forcing the model.
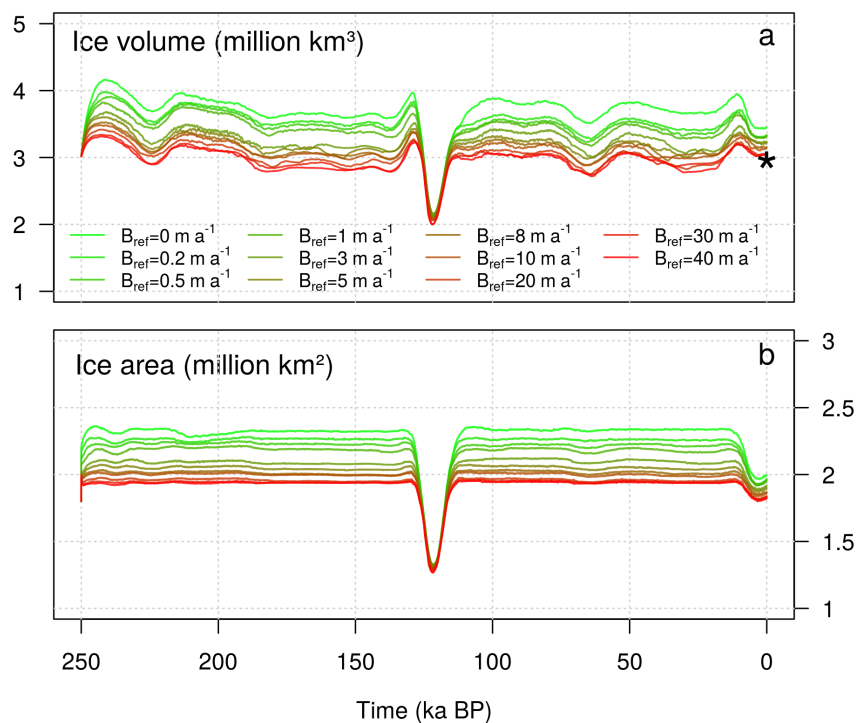
Figure 2. Time evolution of (a) grounded ice volume [million km^3] and (b) ice-covered area [million km^2] simulated for different values of B_{ref} (m a^{-1}) having set $\kappa = 0$ (see Table 1). The star at 0 ka BP shows the present-day estimated volume of the GrIS (Bamber et al., 2013).
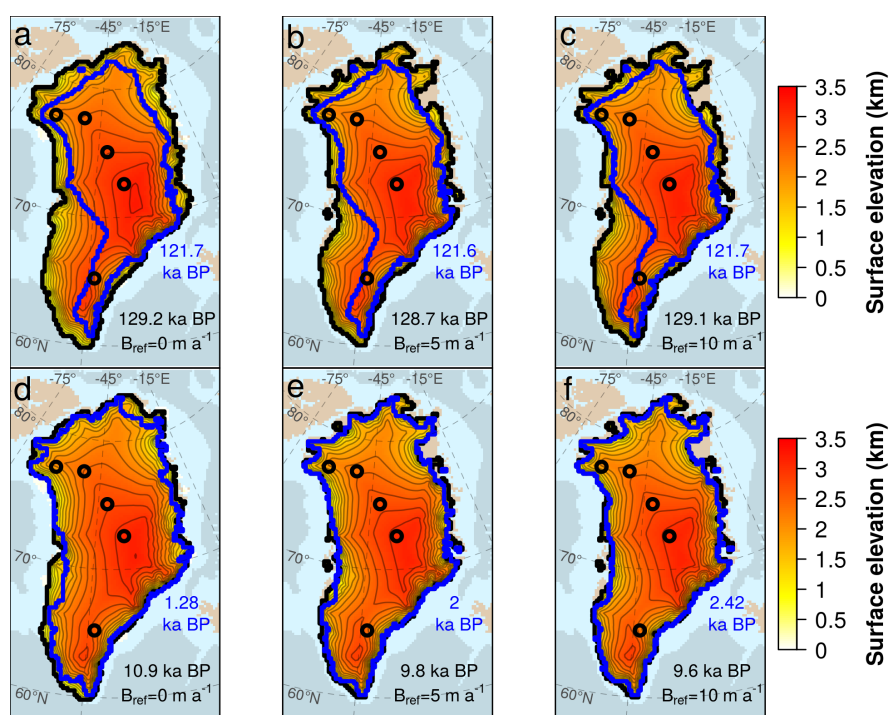
Figure 3. Maximum GrIS surface elevation (km) simulated at Termination II (a-c) and Termination I (d-f) for different values of the reference basal melting rate $B_{\mathrm{ref}} = 0, 5, 10\,\mathrm{m\,a^{-1}}$ under constant oceanic conditions ($\kappa = 0$). The timing at which the ice volume reaches its maximum value during a glacial cycle depends on the experiment and is stated in black for each snapshot. Blue lines indicate the GrIS extension at the following peak of deglaciation with its corresponding timing reported in blue. Black circles indicate the locations of the Camp Century, NEEM, NGRIP, GRIP and Dye3 ice-cores (from North to South).
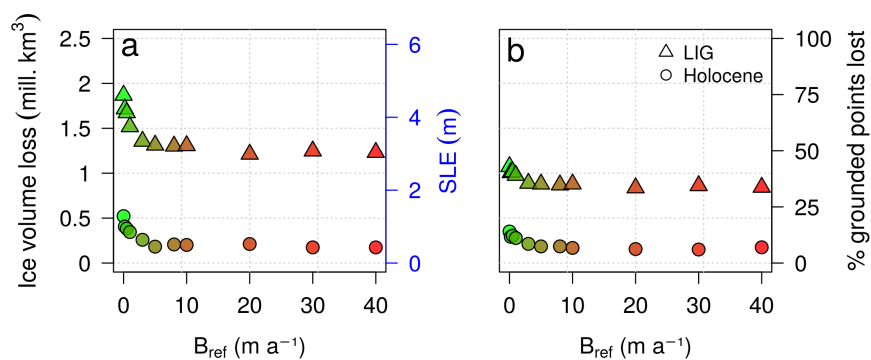
Figure 4. Distribution of the ice volume (a) and percentage of grounded points (b) lost during the LIG (triangles) and the Holocene (circles) as a function of B_{ref}. The loss is calculated between the time at which the ice volume reaches its maximum value simulated before the deglaciation (between 130 and 128 ka BP for TII and between 11 and 9 ka BP for TI) and its following ice minimum (between 122 and 121 ka BP for the Eemian and between 8 and 0 ka BP for the Holocene). The colors of the points follow the legend of Fig. 2 for clarity.
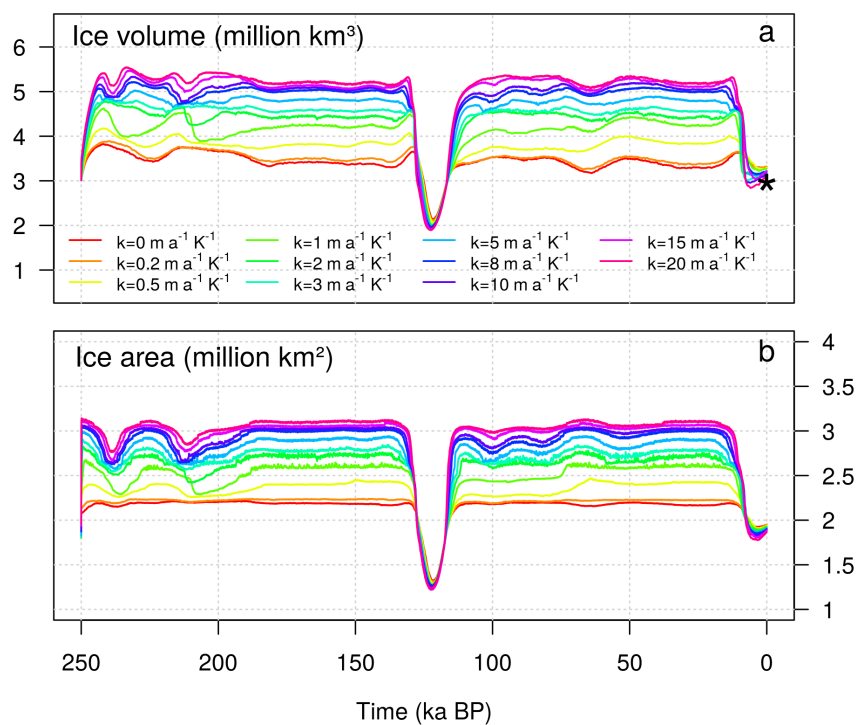
Figure 5. (a) Time evolution of GrIS grounded ice volume [million km^3] and (b) ice area [million km^2] simulated for different values of the heat-flux coefficient κ, having set $B_{\mathrm{ref}} = 1$ m a^{-1}. The star shows to the GrIS ice volume estimated for the present day (Bamber et al., 2013).
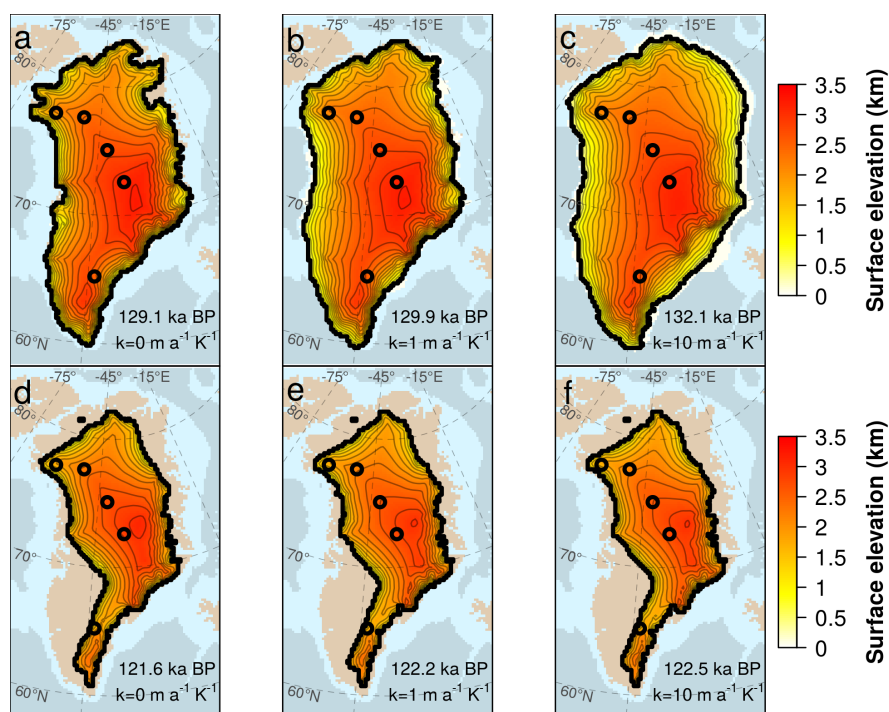
Figure 6. (a-c) Maximum (TII) and (d-f) minimum (Eemian) GrIS ice distribution simulated for three values of the melting rate sensitivity κ having set $B_{\text{ref}} = 1$ m a^{-1}. The timing of these snapshots depends on the experiment and is stated in black for each snapshot. Black lines represent simulated grounding line positions. Black circles indicate the locations of the Camp Century, NEEM, NGRIP, GRIP and Dye3 ice-cores (from North to South).
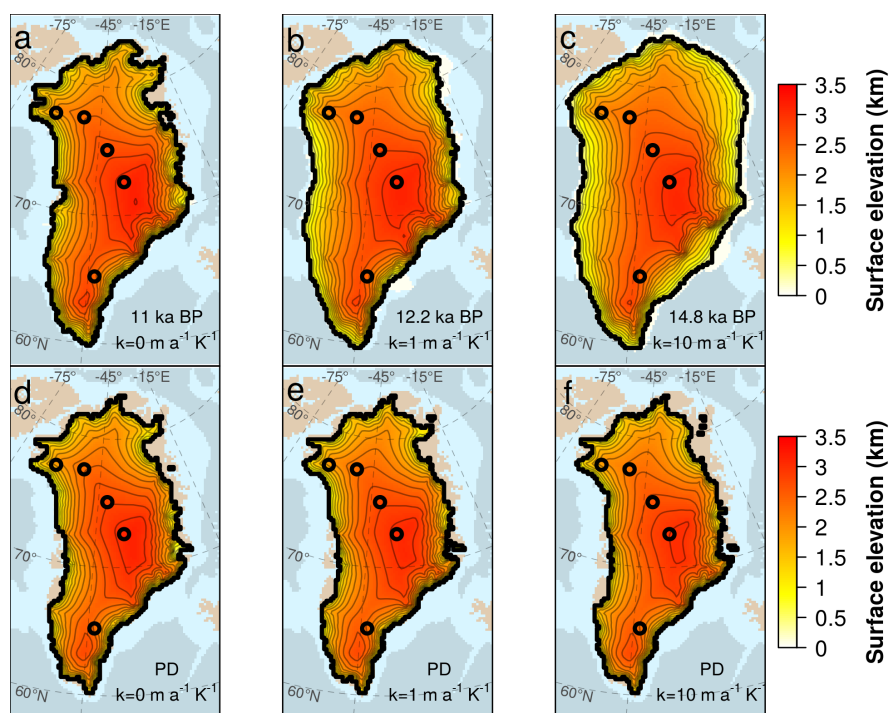
Figure 7. (a-c) TI and (d-f) present-day GrIS ice distribution simulated for three values of the heat-flux coefficient κ having set $B_{\mathrm{ref}} = 1$ m a^{-1}. The timing of the snapshots depends on the experiment and is stated. Black lines represent simulated grounding line positions. Black circles indicate the locations of the Camp Century, NEEM, NGRIP, GRIP and Dye3 ice-cores (from North to South).
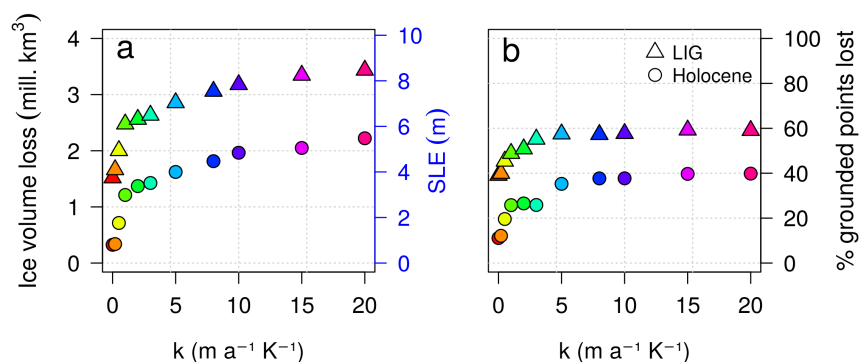
Figure 8. Distribution of ice volume (a) and percentage of grounded points (b) lost during the LIG and the Holocene as a function of κ, for $B_{\mathrm{ref}} = 1$ m a^{-1}. The loss is calculated between the time at which the ice volume reaches its maximum value simulated before deglaciation (between 140 and 128 ka BP for TII and between 19 and 10 ka BP for TI) and the subsequent ice minimum (between 122 and 121 ka BP for the Eemian and between 8 and 0 ka BP for the Holocene). The colors of the points follow the legend of Fig. 5 for clarity.
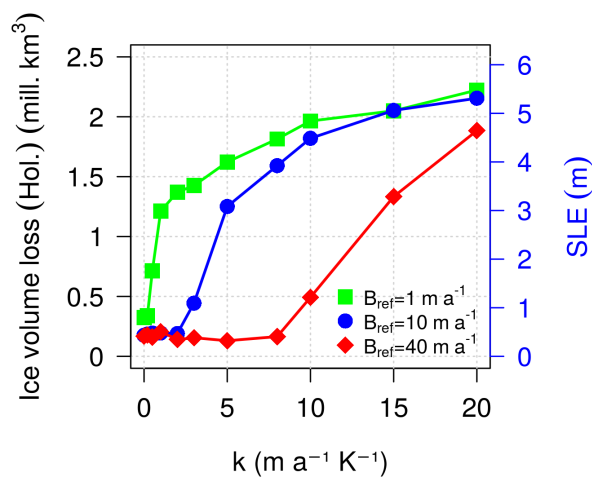
Figure 9. Distribution of the ice volume lost in the Holocene as a function of the heat-flux coefficient κ, simulated for three selected reference basal melting rates ($B_{ref} = 1, 10, 40 \, \mathrm{m \, a^{-1}}$). The ice volume loss is calculated between the time at which the ice volume reaches its maximum value before the deglaciation and the present day. The green points are the same as the circles of Fig. 8 a (for the Holocene).
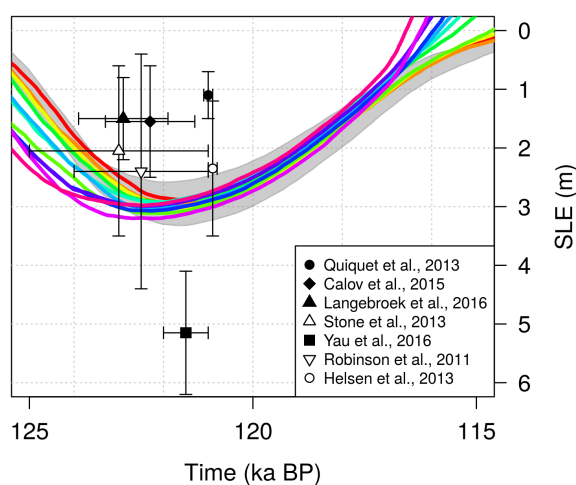
Figure 10. GrIS ice volume evolution simulated for different values of the melting rate sensitivity κ during the last interglacial (see Fig. 5 for the line colour legend). The ice volumes have been converted to values of SLE anomaly with respect to the present-day volumes estimated in each specific simulation. Grey shading represents the reference basal melting rates B_{ref} investigated for the case of constant in time oceanic forcing ($\kappa = 0 \ \mathrm{m\,a}^{-1}\,\mathrm{K}^{-1}$). Black and white symbols indicate the LIG minimum ice volumes estimated by previous studies. The tight clustering of our estimates compared to previous work is due to the fact that the sole uncertainty is here related to the oceanic forcing through κ.
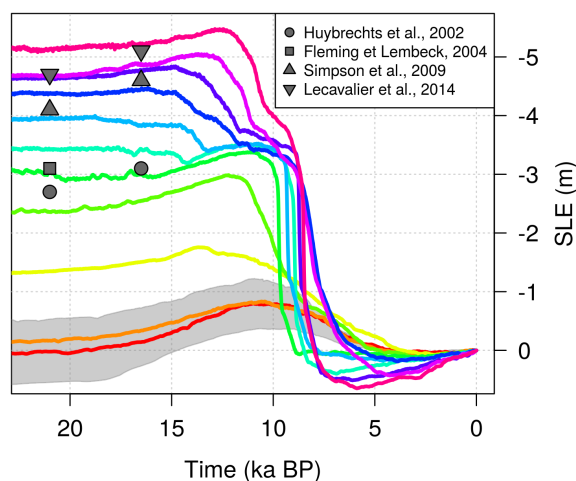
Figure 11. GrIS sea-level evolution simulated for different values of the melting rate sensitivity κ during the last deglaciation (see Fig. 5 for the line colour legend). The ice volumes have been converted to values of SLE anomaly with respect to the present-day volumes estimated in each specific simulation. As in Fig. 10, grey shading represents the simulations for the different reference basal melting rates B_{ref} investigated for the case of constant in time oceanic forcing ($\kappa = 0$). Grey dots indicate estimates of the GrIS ice volume at the LGM (21 ka BP) and of the maximum ice volume reached before the last deglaciation (16.5 ka BP) as suggested by previous work.
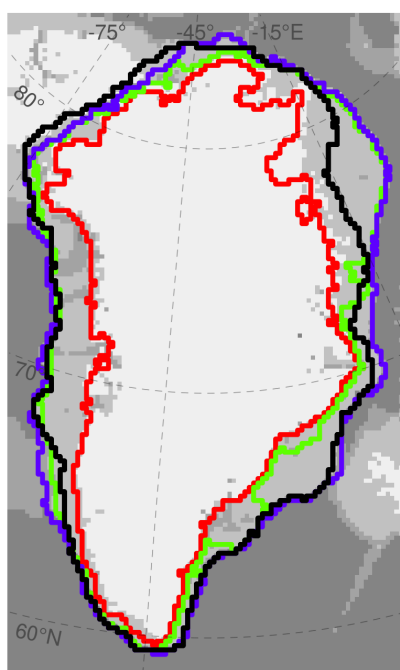
Figure 12. GrIS total extent (ice shelves are included) simulated at the LGM (21 ka BP) for three particular values of the melting rate sensitivity $\kappa = 0$, 1 and 10 m a^{-1} K^{-1} (red, green and purple lines, respectively), having set $B_{\text{ref}} = 1$ m a^{-1}. LGM GrIS grounding line position estimated by (Lecavalier et al., 2014) is shown for comparison (black line).
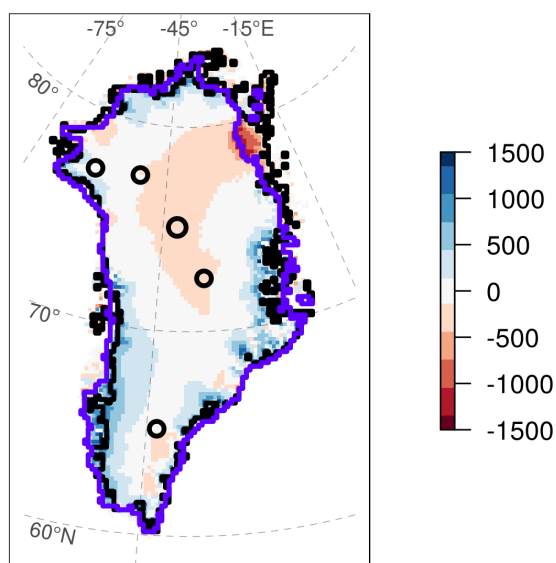
Figure 13. Modelled minus observed surface elevation for the present day. Modelled data are taken from the GRISLI-UCM simulation which best estimates the presumed LGM extension ($B_{\mathrm{ref}} = 1 \ \mathrm{m \ a^{-1}}$ and $\kappa = 10 \ \mathrm{m \ a^{-1} \ K^{-1}}$) while the observed surface elevation is taken from Bamber et al. (2013). Purple and black lines represent simulated and observed GrIS extensions, respectively. Black circles indicate the locations of the Camp Century, NEEM, NGRIP, GRIP and Dye3 ice-cores (from North to South).